Cite as: Solomon *et al.*, *Science* 10.1126/science.aae0061 (2016).

Emergence of healing in the Antarctic ozone layer

Susan Solomon,[1]* Diane J. Ivy,[1] Doug Kinnison,[2] Michael J. Mills,[2] Ryan R. Neely III,[3,4] Anja Schmidt[3]

[1]Department of Earth, Atmospheric, and Planetary Science, Massachusetts Institute of Technology, Cambridge, MA 02139, USA. [2]Atmospheric Chemistry Observations and Modeling Laboratory, National Center for Atmospheric Research, PO Box 3000, Boulder, CO 80305, USA. [3]School of Earth and Environment, University of Leeds, Leeds, UK. [4]National Centre for Atmospheric Science, University of Leeds, Leeds, UK.

*Corresponding author. Email: solos@mit.edu

Industrial chlorofluorocarbons that cause ozone depletion have been phased out under the Montreal Protocol. A chemically-driven increase in polar ozone (or "healing") is expected in response to this historic agreement. Observations and model calculations taken together indicate that the onset of healing of Antarctic ozone loss has now emerged in September. Fingerprints of September healing since 2000 are identified through (i) increases in ozone column amounts, (ii) changes in the vertical profile of ozone concentration, and (iii) decreases in the areal extent of the ozone hole. Along with chemistry, dynamical and temperature changes contribute to the healing, but could represent feedbacks to chemistry. Volcanic eruptions episodically interfere with healing, particularly during 2015 (when a record October ozone hole occurred following the Calbuco eruption).

Antarctic ozone depletion has been a focus of attention by scientists, policymakers and the public for three decades (*1*). The Antarctic "ozone hole" opens up in austral spring of each year, and is measured both by its depth (typically a loss of about half of the total integrated column amount) and its size (often more than 20 million km^2 in extent by October). Ozone losses have also been documented in the Arctic, and at mid-latitudes in both hemispheres (*2*). Concern about ozone depletion prompted a worldwide phase-out of production of anthropogenic halocarbons containing chlorine and bromine, known to be the primary source of reactive halogens responsible for the depletion (*2*). The ozone layer is expected to recover in response, albeit very slowly, due mainly to the long atmospheric residence time of the halocarbons responsible for the loss (*2*).

Ozone recovery involves multiple stages, starting with (i) a reduced rate of decline, followed by (ii) a leveling off of the depletion, and (iii) an identifiable ozone increase that can be linked to halocarbon reductions (*2*, *3*). For simplicity, we refer to the third stage of recovery as healing. All three stages of recovery have been documented in the upper stratosphere in mid- and low-latitudes, albeit with uncertainties (*2*, *4–6*). Some studies provide evidence for all three recovery stages in ozone columns at mid-latitudes, despite dynamical variability (*7*). While the first and second stages of Antarctic and Arctic recovery have also been well documented (*8–10*), recent scientific assessment concluded that the emergence of the third stage had not been established by previous studies of the polar regions (*2*). Further, in October of 2015 the Antarctic ozone hole reached a record size (*11*), heightening questions about whether any signs of healing can be identified in either polar region.

Controls on polar ozone

Polar ozone depletion is driven by anthropogenic chlorine and bromine chemistry linked to halocarbon emissions (*2*, *12*). But ozone is not expected to heal in a monotonic fashion as halocarbon concentrations decrease, due to confounding factors (such as meteorological changes) that induce variability from one year to another and could influence trends (*2*, *13*, *14*).

The exceptionally large ozone depletion in the polar regions compared to lower latitudes involves polar stratospheric cloud (PSC) particles that form under cold conditions. These clouds drive heterogeneous chlorine and bromine chemistry that is sensitive to small changes in temperature (and hence to meteorological variability). A related and second factor is change in the transport of ozone and other chemicals by circulation or mixing changes (*2*). Further, some PSCs, as well as aerosol particles capable of driving similar chemistry, are enhanced when volcanic eruptions increase stratospheric sulfur. Significant volcanic increases in Antarctic ozone depletion were documented in the early 1990s following the eruption of Mount Pinatubo in 1991, and are well simulated by models (*15*, *16*). Since about 2005, a series of smaller-magnitude volcanic eruptions has increased stratospheric particle abundances (*17*, *18*), but the impact of these on polar ozone recovery has not previously been estimated.

Observations and model test cases

We examine healing using balloon ozone data from the Syowa and South Pole stations. We also use total ozone column measurements from South Pole and the Solar Backscatter Ultra-Violet satellite (SBUV; here we average SBUV data over the region from 63°S to the polar edge of

coverage). The SBUV record has been carefully calibrated and compared to suborbital data (*19*). We also employ the Total Ozone Mapping Spectrometer/Ozone Monitoring Instrument merged dataset for analysis of the horizontal area of the ozone hole (TOMS/OMI; *20*). Calibrated SBUV data are currently only available to 2014, while the other records are available through 2015 (affecting the time intervals evaluated here). Model calculations are carried out with the Community Earth System Model (CESM1) Whole Atmosphere Community Climate Model (WACCM), which is a fully coupled state-of-the-art interactive chemistry climate model (*21*). We use the specified dynamics option, SD-WACCM, where meteorological fields including temperature and winds are derived from observations (*22*, *23*). The analysis fields allow the time-varying temperature-dependent chemistry that is key for polar ozone depletion to be simulated. The model's ability to accurately represent polar ozone chemistry has recently been documented (*23*, *24*). Aerosol properties are based on the Chemistry and Climate Model Intercomparison (CCMI) recommendation (*25*) or derived inline from a version of WACCM that uses a modal aerosol sub-model (*23*, *26*). The modal sub-model calculates variations in stratospheric aerosols using a database of volcanic SO_2 emissions and plume altitudes based on observations (table S1) along with non-volcanic sulfur sources (particularly OCS, anthropogenic SO_2, and dimethyl sulfide). The injection heights and volcanic inputs are similar to previous studies (*18*, *27*) and the calculated aerosol distributions capture the timing of post-2005 eruptions observed by several tropical, mid- and high-latitude lidars, and satellite climatologies (*26*). Based on comparisons to lidar data for several eruptions and regions (*26*), our modeled post-2005 total stratospheric volcanic aerosol optical depths are estimated to be accurate to within ±40% (see supplement). Differences between the CCMI aerosol climatology and our calculated modal aerosol model results can be large, especially in the lower stratosphere (*26*), and can affect ozone abundances.

The concentrations of halogenated gases capable of depleting ozone peaked in the polar stratosphere around the late 1990s due to the Montreal Protocol, and are slowly declining (*2*, *28*). We analyze what role these decreases in halogens play in polar ozone trends since 2000 along with other drivers of variability and change. The year 2002 displayed anomalous meteorological behavior in the Antarctic (*29*), and it is excluded from all trend analyses throughout this paper.

Three different model simulations are used to examine drivers of polar ozone changes since 2000, using full chlorine and bromine chemistry in all cases but employing (i) observed time-varying changes in temperature and winds from meteorological analyses, with calculated background and volcanic stratospheric particles as well as other types of PSCs (Chem-Dyn-Vol), (ii) a volcanically clean case (Vol-Clean, considering only background sources of stratospheric sulfur), as well as (iii) a chemistry-only case in which annual changes in all meteorological factors (including the temperatures that drive chemistry) are suppressed by repeating conditions for 1999 throughout, and volcanically clean aerosols are imposed (Chem-Only). The Antarctic stratosphere in austral spring of 1999 was relatively cold and was deliberately chosen for large chemical ozone losses. A longer run using full chemistry and CCMI aerosols illustrates the model's simulation of the onset of ozone loss since 1979. Further information on statistical approaches, methods, datasets, and model are provided in the supplement.

Our Chem-Only simulation probably represents a conservative estimate of what may reasonably be considered to be chemical effects, because it does not include radiatively-driven temperature changes that are expected to occur due to changes in ozone (*30*) and their feedback to chemical processes. Temperatures and ozone are coupled because absorption of sunlight by ozone heats the stratosphere. If ozone increases due to reductions in halogens, then temperatures will increase, which feeds back to the chemistry (for example, by reducing the rate of temperature-dependent heterogeneous reactions that deplete ozone), further increasing ozone. Such effects have not been separated here from other changes in temperature or in winds (due to dynamical variability or forcings such as greenhouse gases).

Antarctic ozone trends, variability, and fingerprints of healing

Most analyses of Antarctic ozone recovery to date consider October or Sep-Oct-Nov averages (*7*, *9*, *10*). The historic discovery of the Antarctic ozone hole was based on observations taken in October (*1*), and healing cannot be considered complete until the ozone hole ceases to occur in that month, around mid-century (*2*, *28*). However, October need not be the month when the onset of the healing process emerges. A first step in understanding whether a 'signal' of the onset of healing can be identified is examining trends and their statistical significance relative to the 'noise' of interannual variability.

October displays the deepest ozone depletion of any month in the Antarctic. However, it is subject to large variability due to seasonal fluctuations in temperature and transport, as well as volcanic aerosol chemistry. Figure 1 shows the time series of measured Antarctic October total ozone obtained from SBUV and South Pole data along with the model calculations; tables S2 and S3 provide the associated post-2000 trends and 90% confidence intervals. Figure 1 shows that SD-WACCM reproduces the observed October variability from year to year when all factors are considered (Chem-Dyn-Vol). However, the October total ozone trends

are not yet positive with 90% certainty in the data, nor in the model. In contrast, other months displaying smaller depletion but reduced variability (particularly September; see Fig. 1, fig. S1, and tables S2 and S3) reveal positive ozone trends over 2000-2014 that are statistically significant at 90% confidence in SBUV and station measurements. Arctic ozone has long been known to be more variable than the Antarctic (*2*), and no Arctic month yet reveals a significant positive trend in either the Chem-Dyn-Vol model or the SBUV observations when examined in the same manner (table S2).

The September profile of balloon ozone trends is a key test of process understanding. Figure 2 shows measured balloon profile trends for the South Pole and Syowa stations for 2000-2015, together with WACCM model simulations. The large ozone losses measured at Syowa as the ozone hole developed from 1980-2000 are also shown for comparison. Antarctic station data need to be interpreted with caution due to an observed long-term shift in the position of the Antarctic vortex that affects Syowa in particular in October; South Pole is however, less influenced by this effect (*31*). The ozonesonde datasets suggest clear increases since 2000 between about 100 and 50 hPa (*10*). The simulation employing chemistry alone with fixed temperatures yields about half of the observed healing, with the remainder in this month being provided by dynamics/temperature. The simulations also suggest a negative contribution (offset to healing) due to volcanic enhancements of the ozone depletion chemistry between about 70 and 200 hPa (see fig. S2 showing similar effects in other months in this sensitive height range). The comparisons to the model trend profiles in Fig. 2 provide an important fingerprint that the Antarctic ozone layer has begun to heal in September. This is consistent with basic understanding that reductions in ozone depleting substances in the troposphere will lead to healing of polar ozone that emerges over time, with lags due to the transport time from the troposphere to the stratosphere along with the time required for chemically-driven trends to become significant compared to dynamical and volcanic variability.

The seasonal cycle of monthly total ozone trends from the SBUV satellite is displayed in Fig. 3, along with model calculations for various cases. The contributions to the modeled trends due to volcanic inputs (difference between Chem-Dyn-Vol and Vol-Clean simulations), chemistry alone, and dynamics/temperature (difference between Vol-Clean and Chem-Only simulations) are shown in the lower panel. While it is not possible to be certain that the reasons for variations obtained in the observations are identical to those in the model, the broad agreement of the seasonal cycle of total trends in SBUV observations and the model calculations supports the interpretation here. Less dynamical variability in September compared to October (as shown by smaller error bars on the dynamics/temperature term in Fig. 3, bottom panel) along with strong chemical recovery make September the month when the Antarctic ozone layer displays the largest amount of healing since 2000. The data suggest September increases at 90% confidence of 2.5 ± 1.6 DU per year over the latitudes sampled by SBUV and 2.5 ± 1.5 DU per year from the South Pole sondes. These values are consistent with the Chem-Dyn-Vol model values of 2.8 ± 1.6 and 1.9 ± 1.5 DU per year, respectively. Because the model simulates much of the observed year-to-year variability in September total ozone well for both the South Pole and for SBUV observations, confidence is enhanced that there is a significant chemical contribution to the trends (Fig. 1). As a best estimate, the model results suggest that roughly half of the September column healing is chemical, while half is due to dynamics/temperature though highly variable. The modeled total September healing trend has been reduced by about 10% due to the chemical effects of enhanced volcanic activity in the latter part of 2000-2014.

Volcanic eruptions affect polar ozone depletion because injections of sulfur enhance the surface areas of liquid PSCs and aerosol particles (*32*). Higher latitude eruptions directly influence the polar stratosphere but tropical eruptions can enhance polar aerosols following transport. The model indicates that numerous moderate eruptions since about 2005 have affected polar ozone in both hemispheres (see table S1 for eruptions, dates, and latitudes), particularly at pressures from about 70-300 hPa (Fig. 4). At pressures above about 100 hPa, temperatures are generally too warm for many PSCs to form, but there is sufficient water that effective heterogeneous chemistry can take place under cold polar conditions (*12*). Peak volcanic losses locally as large as 30% and 55% are calculated in the Antarctic in 2011 and 2015, mainly due to the Chilean eruptions of Puyehue-Cordón Caulle and Calbuco, respectively; volcanic contributions to depletions tracing to tropical eruptions are also obtained in several earlier years. At these pressures, contributions to the total column are small but significant: the integrated additional Antarctic ozone column losses averaged over the polar cap are between 5 and 13 Dobson Units following the respective eruptions shown in Fig. 4.

The ozone hole typically begins to open in August each year and reaches its maximum areal extent in October. Decreases in the areal extent of the October hole are expected to occur in the 21st century as chemical destruction slows, but cannot yet be observed against interannual variability, in part because of the extremely large hole in 2015 (fig. S3). But monthly averaged observations in September display shrinkage of 4.5 ± 4.1 million km^2 over 2000-2015 (Fig. 5, left panel). The model underestimates the observed September hole size by about 15% on average, but yields similar variability (Fig. 5) and trends (4.9 ± 4.7 million km^2). The right

panel of Fig. 5 shows that the observed and modeled day of year when the ozone hole exceeds a threshold value of 12 million km^2 is occurring later in recent years, indicating that early September holes are becoming smaller (see Fig. 6). This result is robust to the specific choice of threshold value, and implies that the hole is opening more slowly as the ozone layer heals. The Chem-Only model results in Fig. 5 show that if temperatures, dynamical conditions, and volcanic inputs had remained the same as 1999 until now, the September ozone hole would have shrunk by about 3.5 ± 0.3 million km^2 due to reduced chlorine and bromine, dominating the total shrinkage over this period.

Volcanic eruptions caused the modeled area of the September average ozone holes to expand substantially in several recent years. Our results as shown in Fig. 5 (left panel) indicate that much of the statistical uncertainty in the observed September trend is not random, but is due to the expected chemical impacts of these geophysical events. In 2006, 2007, and 2008, model calculations suggest that the September ozone holes were volcanically enhanced by about 1 million km^2. The size of the September ozone holes of 2011 and 2015 are estimated to have been, respectively, about 1.0 million km^2 and 4.4 million km^2 larger due to volcanoes (especially Puyehue-Cordón Caulle in 2011 and Calbuco in 2015) than they would otherwise have been, substantially offsetting the chemical healing in those years.

Figure 6 shows that the bulk of the seasonal growth of the ozone hole typically occurs between about days 230 and 250 (late August to early September). As the ozone layer heals, the growth of the hole is expected to occur later in the year (middle and bottom panels), in agreement with observations (top). The slower rates of early season growth are key to the trend of shrinkage of the September averaged ozone hole. For example, the rate of ozone loss depends strongly upon the ClO concentration, so that reduced chlorine concentrations imply slower rates of ozone loss after polar sunrise. The ozone hole of 2015 was considerably larger than ever previously observed over several weeks in October of 2015 (but notably, not in September), and this behavior is well reproduced in our model only when the eruption of Calbuco is considered (figs. S3 and S4). The record-large monthly averaged ozone hole in October 2015 measured 25.3 million km^2, which was 4.8 million km^2 larger than the previous record year (20.6 million km^2 in 2011). When volcanic aerosols are included in the Chem-Dyn-Vol simulation, our calculated monthly averaged October 2015 ozone hole is 24.6 million km^2, while the corresponding value in the volcanically clean simulation is much smaller, 21.1 million km^2 (fig. S3). Therefore, our calculations indicate that cold temperatures and dynamics alone made a much smaller contribution to establishing the October 2015 record than the volcanic aerosols (see figs. S3 and S4), and the cold temperatures are expected to be at least partly a feedback to the volcanically-enhanced large ozone losses. Further, the conclusion that the volcanic aerosols were the dominant cause of the record size of the October 2015 ozone hole would hold based on our calculations even if the volcanic aerosol amounts were overestimated by a factor of several (a much larger error than indicated by our comparison of the model to lidar data for multiple eruptions in *26*, see supplement).

The reason or reasons for the dynamics/temperature contributions to healing of the Antarctic ozone layer are not clear. The dynamical/temperature contributions to healing estimated in Fig. 3 vary by month in a manner that mirrors the ozone depletion in spring, suggesting linkages to the seasonality of the depletion itself and hence possible dynamical feedbacks. Some models (*33*–*35*) suggest that a reduction in transport of ozone to the Antarctic occurred as depletion developed in the 1980s and 1990s, which would imply a reversal and hence enhanced healing as ozone rebounds. But others indicate that ozone depletion increased the strength of the stratospheric overturning circulation (*36*); and a reversal of this factor during recovery would impede healing. While there is robust agreement across models that climate change linked to increasing greenhouse gases should act to increase the strength of the stratospheric overturning circulation, observations show mixed results (*37*); further, the seasonality has not been established, and the magnitude in the Antarctic is uncertain. Internal variability of the climate system linked for example to variations in El Nino could also affect the trends.

Conclusion

After accounting for dynamics/temperature and volcanic factors, the fingerprints presented here indicate that healing of the Antarctic ozone hole is emerging. Our results underscore the combined value of balloon and satellite ozone data, as well as volcanic aerosol measurements together with chemistry-climate models to document the progress of the Montreal Protocol in recovery of the ozone layer.

REFERENCES AND NOTES

1. J. C. Farman, B. G. Gardiner, J. D. Shanklin, Large losses of total ozone in Antarctica reveal seasonal ClO_x/NO_x interaction. *Nature* **315**, 207–210 (1985). doi:10.1038/315207a0
2. World Meteorological Organization/United Nations Environment Programme (WMO/UNEP), *Scientific Assessment of Ozone Depletion: 2014* (Global Ozone Research and Monitoring Project Report No. 55, WMO, 2014).
3. D. J. Hofmann, S. J. Oltmans, J. M. Harris, B. J. Johnson, J. A. Lathrop, Ten years of ozonesonde measurements at the south pole: Implications for recovery of springtime Antarctic ozone. *J. Geophys. Res.* **102**, 8931–8943 (1997). doi:10.1029/96JD03749
4. M. J. Newchurch, E.-S. Yang, D. M. Cunnold, G. C. Reinsel, J. M. Zawodny, J. M. Russell III, Evidence for slowdown in stratospheric ozone loss: First stage of ozone recovery. *J. Geophys. Res.* **108**, 4507 (2003). doi:10.1029/2003JD003471

5. N. R. P. Harris, B. Hassler, F. Tummon, G. E. Bodeker, D. Hubert, I. Petropavlovskikh, W. Steinbrecht, J. Anderson, P. K. Bhartia, C. D. Boone, A. Bourassa, S. M. Davis, D. Degenstein, A. Delcloo, S. M. Frith, L. Froidevaux, S. Godin-Beekmann, N. Jones, M. J. Kurylo, E. Kyrölä, M. Laine, S. T. Leblanc, J.-C. Lambert, B. Liley, E. Mahieu, A. Maycock, M. de Mazière, A. Parrish, R. Querel, K. H. Rosenlof, C. Roth, C. Sioris, J. Staehelin, R. S. Stolarski, R. Stübi, J. Tamminen, C. Vigouroux, K. A. Walker, H. J. Wang, J. Wild, J. M. Zawodny, Past changes in the vertical distribution of ozone – Part 3: Analysis and interpretation of trends. *Atmos. Chem. Phys.* **15**, 9965–9982 (2015). doi:10 5194/acp-15-9965-2015
6. F. Tummon, B. Hassler, N. R. P. Harris, J. Staehelin, W. Steinbrecht, J. Anderson, G. E. Bodeker, A. Bourassa, S. M. Davis, D. Degenstein, S. M. Frith, L. Froidevaux, E. Kyrölä, M. Laine, C. Long, A. A. Penckwitt, C. E. Sioris, K. H. Rosenlof, C. Roth, H.-J. Wang, J. Wild, Intercomparison of vertically resolved merged satellite ozone data sets: Interannual variability and long-term trends. *Atmos. Chem. Phys.* **15**, 3021–3043 (2015). doi:10 5194/acp-15-3021-2015
7. T. G. Shepherd, D. A. Plummer, J. F. Scinocca, M. I. Hegglin, V. E. Fioletov, M. C. Reader, E. Remsberg, T. von Clarmann, H. J. Wang, Reconciliation of halogen-induced ozone loss with the total column ozone record. *Nat. Geosci.* **7**, 443–449 (2014). doi:10 1038/ngeo2155
8. E.-S. Yang, D. M. Cunnold, M. J. Newchurch, R. J. Salawitch, M. P. McCormick, J. M. Russell III, J. M. Zawodny, S. J. Oltmans, First stage of Antarctic ozone recovery. *J. Geophys. Res.* **113**, D20308 (2008). doi:10 1029/2007JD009675
9. M. L. Salby, E. Titova, L. Deschamps, Rebound of Antarctic ozone. *Geophys. Res. Lett.* **38**, L09702 (2011). doi:10 1029/2011GL047266
10. J. Kuttippurath, F. Lefèvre, J.-P. Pommereau, H. K. Roscoe, F. Goutail, A. Pazmiño, J. D. Shanklin, Antarctic ozone loss in 1979–2010: First sign of ozone recovery. *Atmos. Chem. Phys.* **13**, 1625–1635 (2013). doi:10 5194/acp-13-1625-2013
11. WMO, "WMO Antarctic Ozone Bulletins: 2015," 2015; www wmo int/pages/prog/arep/WMOAntarcticOzoneBulletins2015 html.
12. S. Solomon, Stratospheric ozone depletion: A review of concepts and history. *Rev. Geophys.* **37**, 275–316 (1999). doi:10 1029/1999RG900008
13. J. Kuttippurath, S. Godin-Beekmann, F. Lefèvre, M. L. Santee, L. Froidevaux, A. Hauchecorne, Variability in Antarctic ozone loss in the last decade (2004–2013): High-resolution simulations compared to Aura MLS observations. *Atmos. Chem. Phys.* **15**, 10385–10397 (2015). doi:10.5194/acp-15-10385-2015
14. N. J. Livesey, M. L. Santee, G. L. Manney, A Match-based approach to the estimation of polar stratospheric ozone loss using Aura Microwave Limb Sounder observations. *Atmos. Chem. Phys.* **15**, 9945–9963 (2015). doi:10 5194/acp-15-9945-2015
15. D. J. Hofmann, S. J. Oltmans, Antarctic ozone during 1992: Evidence for Pinatubo volcanic aerosol effects. *J. Geophys. Res.* **98**, 18555–18561 (1993). doi:10.1029/93JD02092
16. R. W. Portmann, S. Solomon, R. R. Garcia, L. W. Thomason, L. R. Poole, M. P. McCormick, Role of aerosol variations in anthropogenic ozone depletion in the polar regions. *J. Geophys. Res.* **101**, 22991–23006 (1996). doi:10 1029/96JD02608
17. J.-P. Vernier, L. W. Thomason, J.-P. Pommereau, A. Bourassa, J. Pelon, A. Garnier, A. Hauchecorne, L. Blanot, C. Trepte, D. Degenstein, F. Vargas, Major influence of tropical volcanic eruptions on the stratospheric aerosol layer during the last decade. *Geophys. Res. Lett.* **38**, L12807 (2011). doi:10 1029/2011GL047563
18. C. Brühl, J. Lelieveld, H. Tost, M. Höpfner, N. Glatthor, Stratospheric sulfur and its implications for radiative forcing simulated by the chemistry climate model EMAC. *J. Geophys. Res. Atmos.* **120**, 2103–2118 (2015). Medline doi:10.1002/2014JD022430
19. R. D. McPeters, P. K. Bhartia, D. Haffner, G. L. Labow, L. Flynn, The version 8.6 SBUV ozone data record: An overview. *J. Geophys. Res.* **118**, 8032–8039 (2013).
20. W. Chehade, M. Weber, J. P. Burrows, Total ozone trends and variability during 1979–2012 from merged data sets of various satellites. *Atmos. Chem. Phys.* **14**, 7059–7074 (2014). doi:10.5194/acp-14-7059-2014
21. D. R. Marsh, M. J. Mills, D. E. Kinnison, J.-F. Lamarque, N. Calvo, L. M. Polvani, Climate change from 1850 to 2005 simulated in CESM1(WACCM). *J. Clim.* **26**, 7372–7391 (2013). doi:10 1175/JCLI-D-12-00558 1
22. A. Kunz, L. L. Pan, P. Konopka, D. E. Kinnison, S. Tilmes, Chemical and dynamical discontinuity at the extratropical tropopause based on START08 and WACCM analyses. *J. Geophys. Res.* **116**, D24302 (2011). doi:10 1029/2011JD016686
23. Materials and methods are available as supplementary materials on *Science* Online.
24. S. Solomon, D. Kinnison, J. Bandoro, R. R. Garcia, Polar ozone depletion: An update. *J. Geophys. Res.* **120**, 7958–7974 (2015).
25. F. Arfeuille, B. P. Luo, P. Heckendorn, D. Weisenstein, J. X. Sheng, E. Rozanov, M. Schraner, S. Brönnimann, L. W. Thomason, T. Peter, Modeling the stratospheric warming following the Mt. Pinatubo eruption: Uncertainties in aerosol extinction. *Atmos. Chem. Phys.* **13**, 11221–11234 (2013). doi:10 5194/acp-13-11221-2013
26. M. J. Mills, A. Schmidt, R. Easter, S. Solomon, D. E. Kinnison, S. J. Ghan, R. R. Neely III, D. R. Marsh, A. Conley, C. G. Bardeen, A. Gettelman, Global volcanic aerosol properties derived from emissions, 1990-2014, using WACCM5. *J. Geophys. Res.* **121**, 2332–2348 (2015).
27. M. Höpfner, C. D. Boone, B. Funke, N. Glatthor, U. Grabowski, A. Günther, S. Kellmann, M. Kiefer, A. Linden, S. Lossow, H. C. Pumphrey, W. G. Read, A. Roiger, G. Stiller, H. Schlager, T. von Clarmann, K. Wissmüller Sulfur dioxide (SO_2) from MIPAS in the upper troposphere and lower stratosphere 2002–2012. *Atmos. Chem. Phys.* **15**, 7017–7037 (2015). doi:10 5194/acp-15-7017-2015
28. P. A. Newman, E. R. Nash, S. R. Kawa, S. A. Montzka, S. M. Schauffler, When will the Antarctic ozone hole recover? *Geophys. Res. Lett.* **33**, L12814 (2006). doi:10 1029/2005GL025232
29. A. A. Scaife, D. R. Jackson, R. Swinbank, N. Butchart, H. E. Thornton, M. Keil, L. Henderson, Stratospheric vacillations and the major warming over Antarctica in 2002. *J. Atmos. Sci.* **62**, 629–639 (2005). doi:10 1175/JAS-3334 1
30. P. M. Forster, R. S. Freckleton, K. P. Shine, On aspects of the concept of radiative forcing. *Clim. Dyn.* **13**, 547–560 (1997). doi:10 1007/s003820050182
31. B. Hassler, G. E. Bodeker, S. Solomon, P. J. Young, Changes in the polar vortex: Effects on Antarctic total ozone observations at various stations. *Geophys. Res. Lett.* **38**, L01805 (2011). doi:10 1029/2010GL045542
32. A. Tabazadeh, K. Drdla, M. R. Schoeberl, P. Hamill, O. B. Toon, Arctic "ozone hole" in a cold volcanic stratosphere. *Proc. Natl. Acad. Sci. U.S.A.* **99**, 2609–2612 (2002). Medline doi:10.1073/pnas.052518199
33. S. Meul, S. Oberländer-Hayn, J. Abalichin, U. Langematz, Nonlinear response of modeled stratospheric ozone to changes in greenhouse gases and ozone depleting substances in the recent past. *Atmos. Chem. Phys.* **15**, 6897–6911 (2015). doi:10 5194/acp-15-6897-2015
34. P. Braesicke, J. Keeble, X. Yang, G. Stiller, S. Kellmann, N. L. Abraham, A. Archibald, P. Telford, J. A. Pyle, Circulation anomalies in the Southern Hemisphere and ozone changes. *Atmos. Chem. Phys.* **13**, 10677–10688 (2013). doi:10.5194/acp-13-10677-2013
35. F. Li, J. Austin, J. Wilson, The strength of the Brewer–Dobson circulation in a changing climate: Coupled chemistry–climate model simulations. *J. Clim.* **21**, 40–57 (2008). doi:10 1175/2007JCLI1663 1
36. C. McLandress, T. G. Shepherd, Simulated anthropogenic changes in the Brewer–Dobson Circulation, including its extension to high latitudes. *J. Clim.* **22**, 1516–1540 (2009). doi:10 1175/2008JCLI2679 1
37. N. Butchart, The Brewer-Dobson circulation. *Rev. Geophys.* **52**, 157–184 (2014). doi:10 1002/2013RG000448
38. V. Eyring, J.-F. Lamarque, P. Hess, F. Arfeuille, K. Bowman, M. P. Chipperfield, B. Duncan, A. Fiore, A. Gettelman, M. A. Giorgetta, C. Granier, M. Hegglin, D. Kinnison, M. Kunze, U. Langematz, B. Luo, R. Martin, K. Matthes, P. A. Newman, T. Peter, A. Robock, T. Ryerson, A. Saiz-Lopez, R. Salawitch, M. Schultz, T. G. Shepherd, D. Shindell, J. Stähelin, S. Tegtmeier, L. Thomason, S. Tilmes, J.-P. Vernier, D. W. Waugh, P. J. Young, Overview of IGAC/SPARC Chemistry-Climate Model Initiative (CCMI) Community Simulations in Support of Upcoming Ozone and Climate Assessments. *SPARC Newsl.* **40**, 48–66 (2013).
39. M. M. Rienecker, M. J. Suarez, R. Gelaro, R. Todling, J. Bacmeister, E. Liu, M. G. Bosilovich, S. D. Schubert, L. Takacs, G.-K. Kim, S. Bloom, J. Chen, D. Collins, A. Conaty, A. da Silva, W. Gu, J. Joiner, R. D. Koster, R. Lucchesi, A. Molod, T. Owens, S. Pawson, P. Pegion, C. R. Redder, R. Reichle, F. R. Robertson, A. G. Ruddick, M. Sienkiewicz, J. Woollen, MERRA: NASA's Modern-Era Retrospective Analysis for Research and Applications. *J. Clim.* **24**, 3624–3648 (2011). doi:10 1175/JCLI-D-11-00015 1
40. Z. D. Lawrence, G. L. Manney, K. Minschwaner, M. L. Santee, A. Lambert,

Comparisons of polar processing diagnostics from 34 years of the ERA-Interim and MERRA reanalyses. *Atmos. Chem. Phys.* **15**, 3873–3892 (2015). doi:10.5194/acp-15-3873-2015
41. D. Ivy, S. Solomon, H. E. Rieder, Radiative and dynamical influences on polar stratospheric temperature trends. *J. Clim.*, 10.1175/JCLI-D-15-0503.1 (2015). doi:10.1175/JCLI-D-15-0503.1
42. D. E. Kinnison, G. P. Brasseur, S. Walters, R. R. Garcia, D. R. Marsh, F. Sassi, V. L. Harvey, C. E. Randall, L. Emmons, J. F. Lamarque, P. Hess, J. J. Orlando, X. X. Tie, W. Randel, L. L. Pan, A. Gettelman, C. Granier, T. Diehl, U. Niemeier, A. J. Simmons, Sensitivity of chemical tracers to meteorological parameters in the MOZART-3 chemical transport model. *J. Geophys. Res.* **112**, D20302 (2007). doi:10.1029/2006JD007879
43. J. E. Romero, D. Morgavi, F. Arzilli, R. Daga, A. Caselli, F. Reckziegel, J. Viramonte, J. Díaz-Alvarado, M. Polacci, M. Burton, D. Perugini, Eruption dynamics of the 22–23 April 2015 Calbuco Volcano (Southern Chile): Analysis of tephra fall deposits. *J. Volcanol. Geotherm. Res.* **317**, 15–29 (2016). doi:10.1016/j.jvolgeores.2016.02.027
44. Nicarnica Aviation, "Cabulco eruption, April 2015: AIRS Satellite Measurements," 24 April 2015; http://nicarnicaaviation.com/calbuco-eruption-april-2015/#2

ACKNOWLEDGMENTS

We thank Simone Tilmes (NCAR) for help with the MERRA data. DEK and SS were partially supported by NSF FESD grant OCE-1338814 and DI was supported by NSF atmospheric chemistry division grant 1539972. AS was supported by an Academic Research Fellowship from the University of Leeds, an NCAR visiting scientist grant, and Natural Environment Research Council grant NE/N006038/1. The National Center for Atmospheric Research (NCAR) is sponsored by the U.S. National Science Foundation. WACCM is a component of the Community Earth System Model (CESM), which is supported by the National Science Foundation (NSF) and the Office of Science of the U.S. Department of Energy. We are grateful to David Fahey, Birgit Hassler, William Dean McKenna, and the anonymous reviewers for helpful comments. Instructions for access to data reported in this paper are given in the supplement.

SUPPLEMENTARY MATERIALS

www.sciencemag.org/cgi/content/full/science.aae0061/DC1
Materials and Methods
Figs. S1 to S4
Tables S1 to S3
References (*38*–*44*)

6 December 2015; accepted 20 June 2016
Published online 30 June 2016
10.1126/science.aae0061

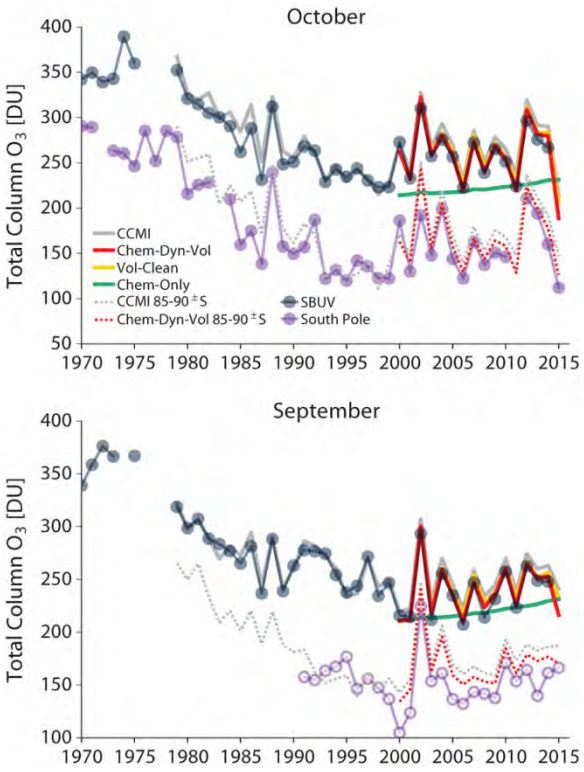

Fig. 1. Monthly averaged Antarctic total ozone column for October and September, from SBUV and South Pole observations and for a series of model calculations. Total ozone data at the geographic South Pole are from Dobson observations where available (filled circles) and balloon sondes (open circles, for September, when there is not sufficient sunlight for the Dobson). SBUV data for each month are compared to model runs averaged over the polar cap latitude band accessible by the instrument, while South Pole data are compared to simulations for 85-90°S.

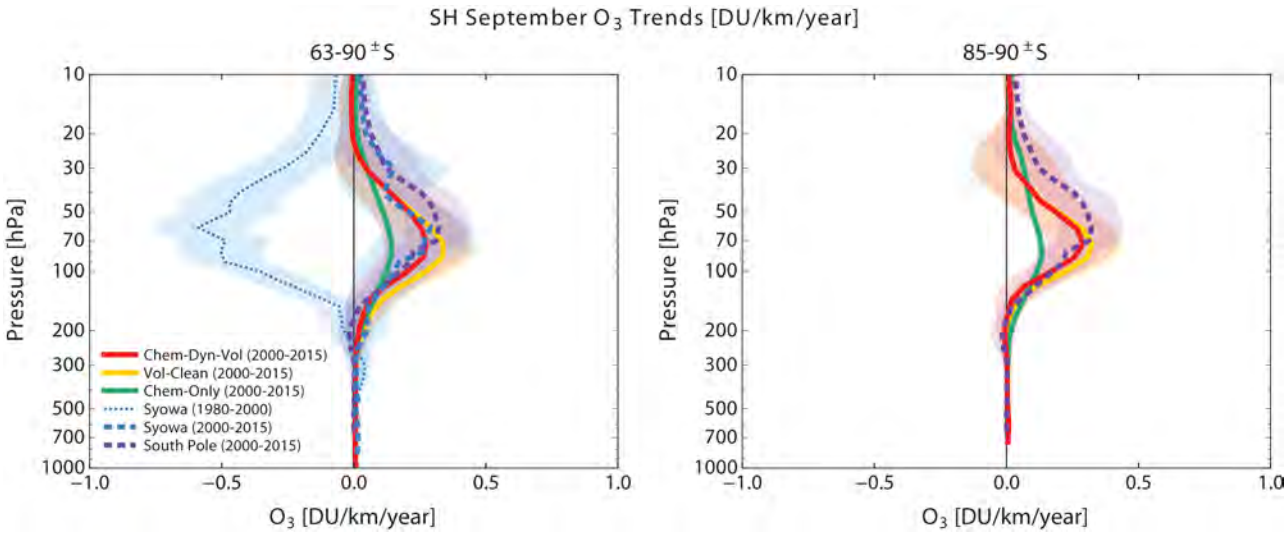

Fig. 2. Trends in September ozone profiles from balloons at Syowa (69°S, 39.58°E, left panel) and South Pole (right panel) stations versus pressure, along with model simulations averaged over the polar cap for the Chem-Dyn-Vol, Vol-Clean, and Chem-Only model simulations. The shading represents the uncertainties on the trends at the 90% statistical confidence interval.

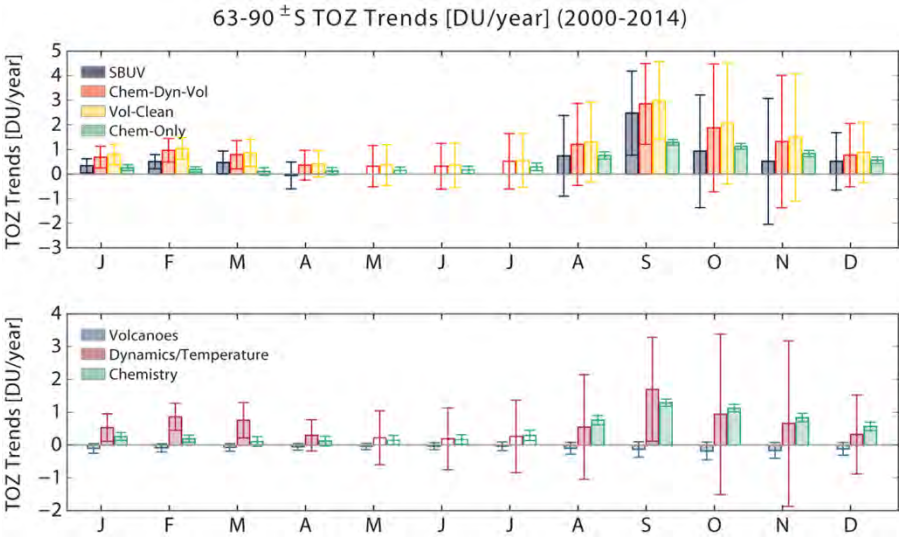

Fig. 3. (top) Trends in total ozone abundance (TOZ) from 2000-2014 by month, from monthly and polar cap averaged SBUV satellite observations together with numerical model simulations masked to the satellite coverage, for the Chem-Dyn-Vol, Vol-Clean, and Chem-Only simulations; error bars denote 90% statistical confidence intervals. (bottom) Contributions to the simulated monthly trends in total ozone abundance driven by dynamics/temperature (from Vol-Clean minus Chem-Only), chemistry only, and volcanoes (from Chem-Dyn-Vol minus Vol-Clean). In austral winter, SBUV measurements do not extend to 63°S, therefore the model averages for those months cover 63-90°S (open bars).

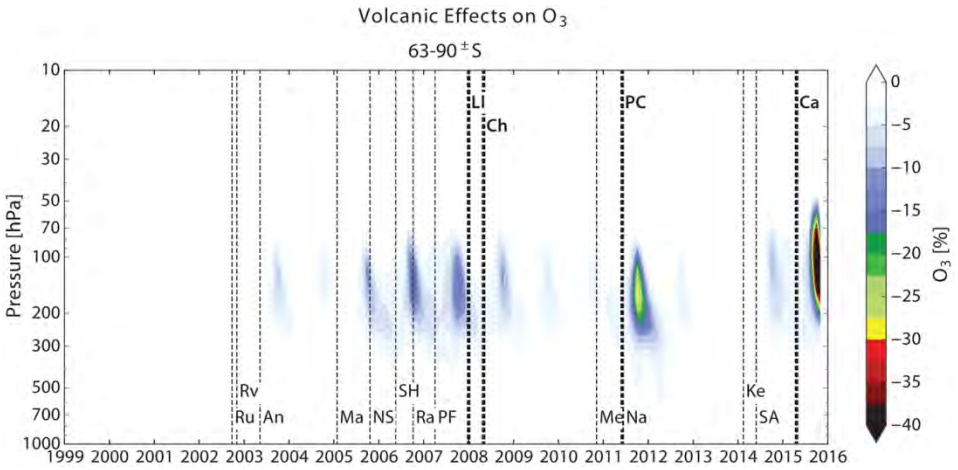

Fig. 4. Model calculated percentage changes in local concentrations of ozone due to a series of moderate volcanic eruptions (from Dyn-Chem-Volc minus Vol-Clean simulations), averaged over the Antarctic polar cap as a function of pressure and month. Volcanic eruptions that have dominated the changes are indicated, with tropical eruptions at the bottom while higher latitude eruptions are shown at the top, where An=Anatahan, Ca=Calbuco, Ch=Chaiten, Ke=Kelut, Ll=Llaima, Ma=Manam, Me=Merapi, Na=Nabro, NS=Negra Sierra, PC= Puyehue-Cordón Caulle, PF=Piton de la Fournaise, Ra=Rabaul (also referred to as Tavurvur), Ru=Ruang, Rv=Reventador, SA=Sangeang Api, SH=Soufriere Hills.

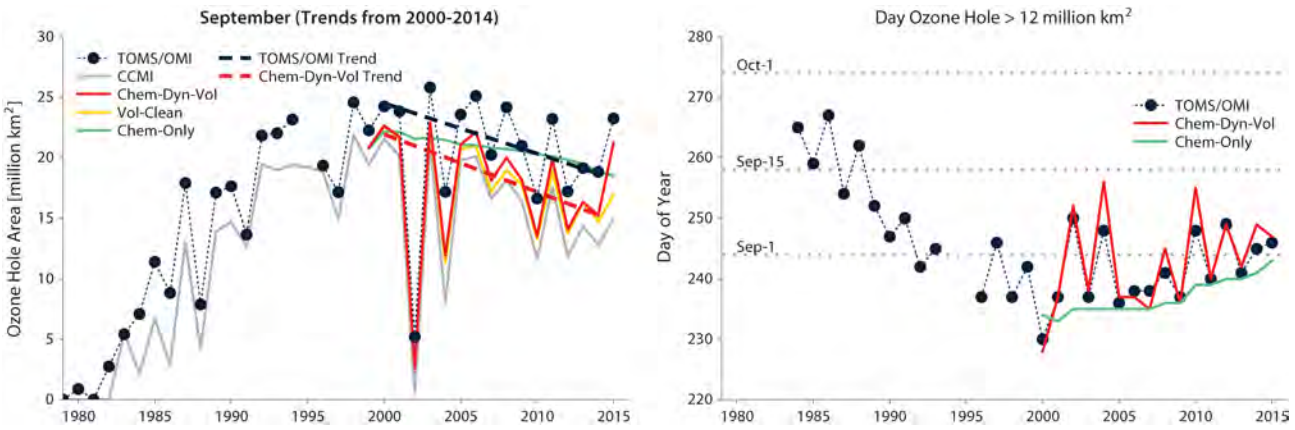

Fig. 5. Annual size of the September monthly average ozone hole (defined as the region where total ozone amount is less than 220 DU, left panel) from TOMS satellite observations together with numerical model simulations for the Chem-Dyn-Vol, Vol-Clean, and Chem-Only simulations. Trends in the TOMS observations (heavy dashed black line) and the Chem-Dyn-Vol model calculations from 2000-2015 (heavy dashed red line) are also indicated. The annual day of year when the size of the ozone hole exceeds 12 million km^2 (and remains above that value for at least 3 days) in the TOMS observations and model simulations are shown in the right panel.

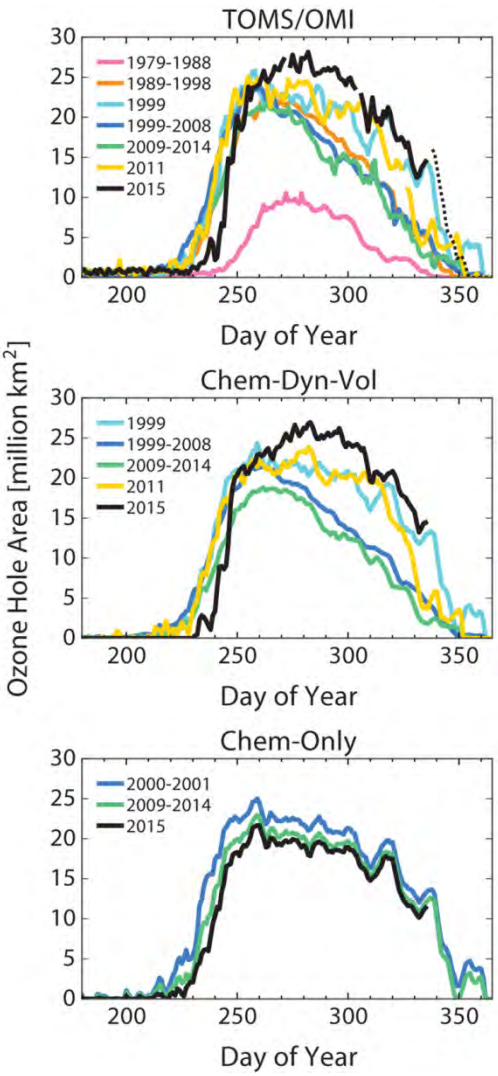

Fig. 6. Daily measurements (top) and model calculations (middle and bottom) of the size of the Antarctic ozone hole versus day of year in different time intervals or years, with 2015 shown in black. Dashed black line in the top panel denotes the 2015 TOMS data after the period covered by the model runs.